Separation Science and Technology
Publication details, including instructions for authors and subscription information:
http://www.informaworld.com/smpp/title~content=t713708471

Modeling of a Continuous Crystallization Process for Solvent Dewaxing

Jun Li[a]; Hao He[a]; Saeed Alaamri[a]; Yuzhong Su[a]
[a] Department of Chemical and Biochemical Engineering, College of Chemistry and Chemical Engineering, Xiamen University, Xiamen, China

To cite this Article Li, Jun , He, Hao , Alaamri, Saeed and Su, Yuzhong(2008) 'Modeling of a Continuous Crystallization Process for Solvent Dewaxing', Separation Science and Technology, 43: 8, 2023 — 2047
To link to this Article: DOI: 10.1080/01496390802064042
URL: http://dx.doi.org/10.1080/01496390802064042

Separation Science and Technology, 43: 2023–2047, 2008

ISSN: 0149-6395 print/1520-5754 online
DOI: 10.1080/01496390802064042

Taylor & Francis
Taylor & Francis Group

Modeling of a Continuous Crystallization Process for Solvent Dewaxing

Jun Li, Hao He, Saeed Alaamri, and Yuzhong Su
Department of Chemical and Biochemical Engineering, College of Chemistry and Chemical Engineering, Xiamen University, Xiamen, China

Abstract: A steady 1-D parallel flow model was established for a continuous solvent dewaxing process; the model equations were numerically solved to obtain the wax supersaturations, amount of crystals, crystal sizes and crystal size distributions in the wax-oil-solvent solution along the flow direction. The effects of the operating conditions, including temperature distributions, multiple dilutions, and the composition of dewaxing solvent, the system's characteristics, including nucleation constant, nucleation order, and wax compound, and the crystallizer dimensions on the formed wax crystals were examined and discussed in detail. The system's nucleation constant was determined by an experimentally obtained recovery of wax; further predictions are in acceptable agreement with the results from a pilot plant.

Keywords: Continuous crystallization; Mathematical modeling; Multiple dilutions; Solvent dewaxing; Temperature distribution

INTRODUCTION

To ensure the fluidity of lubricant oil at low temperature, the long-chain paraffin hydrocarbons (wax) should be removed from the wax-containing oil feedstock; the process is called dewaxing. The technical methods of dewaxing consist of the physicochemical method (e.g., solvent dewaxing, adsorption dewaxing) and the chemical transformation method

Received 24 October 2007; accepted 16 January 2008.
Address correspondence to Jun Li, Department of Chemical and Biochemical Engineering, College of Chemistry and Chemical Engineering, Xiamen University, Xiamen 361005, China. Fax/Tel.: 0086 592 2183055; E-mail: junnyxm@xmu.edu.cn

(e.g., isomerization dewaxing, catalytic dewaxing). Solvent dewaxing is one of the main steps in traditional manufacturing of lube base oil after or before the solvent (furfural) refining process which was modeled in a previous study (1). Furthermore, solvent dewaxing has its advantages such as the variety of feed oil and the valuable byproduct like wax; therefore it cannot be replaced by other technologies although using the chemical method is an inevitable trend in the lubricant industry due to the increasing demand of high-grade base oils.

The principle of solvent dewaxing is simply to take advantage of the high melting point of the long-chain paraffin hydrocarbons that under low temperature can easily crystallize into solid wax crystals through chilling the oil, and then by filtration the solid wax can be separated from the waxy crude oil. It seems that both melt crystallization and solution crystallization take place with regard to the crystal formation mechanism, but the latter one is evidently in dominance due to the decreasing of wax solubility in the bulk oil at low temperature. Usually, dewaxing solvents such as ketone and toluene are used in the process to make filtration easier and improve the recovery of lube oil through meliorating the crystal formation and growth environment and avoiding the formation of crystal networks. For an industrial solvent dewaxing process, some indices, including consumption of energy, filtration rate of the wax-oil-solvent mixture, recovery and pour point of the lube base oil (i.e., the dewaxed oil, DWO), are mainly used for evaluating the process.

It is commonly known that the wax crystal sizes and crystal size distributions (CSDs) consumedly affect these indices aforementioned. In other words, an important issue for the dewaxing process is to study the effect of various operating conditions on the formed wax crystals to improve the traditional solvent dewaxing process. Partly for this purpose, we have built a pilot plant of solvent dewaxing, from which some results under different operating conditions were reported for a vacuum distillate (Omen #3) using methyl ethyl ketone (MEK)-toluene as the dewaxing solvent (2). In this work, we model the process to understand the key factors affecting the crystal formation and growth of wax and direct the pilot-plant operation, because this type of experiment is difficult to carry out and experimental results depend on many factors. Toward the end, we first modeled the continuous crystallization process, then simulated and discussed the effects of various factors, including the operating conditions, characteristics of the system, and crystallizer dimensions on the produced wax crystals. Finally, the calculated recoveries of wax, defined as the amount of precipitated wax crystals divided by the initial wax content in oil feedstock, were compared with available experimental data.

MODEL

As Fig. 1 shows (2), the dewaxing process started by the premixing and preheating of the wax-containing oil and the MEK-toluene dewaxing solvent in a mixing vessel (M). The wax-oil-solvent solution then passed through four tube-in-tube crystallizers (C1-C4) and a mixing (suspension) vessel (S) connected in series for chilling the solution to form wax crystals. Finally, the crystals-containing suspension was separated in a rotary drum filter (F) into solid wax (a slack wax-oil mixture) and oil-solvent solution that should be further separated into desired products. In addition to the dewaxing solvent added before the first crystallizer for the premixing purpose, it could be conveniently fed into the system between the first and the fourth crystallizers as shown in Fig. 1. These dewaxing solvent additions are typically called a multiple dilution process, which will be considered in modeling the process. In the crystallizers, scrapers were installed and rotated with a low speed of about 5 rpm.

In order to simplify mathematical description, assumptions are made as follows:

1. The system between the first and the fourth crystallizers is considered because crystallization could not start until the first crystallizer and the suspension vessel is used as a reservoir for suspensions.
2. The wax-oil-solvent solution passing through the four crystallizers is looked as a steady 1-D parallel flow due to the relatively long route of the fluid. And the effect of the scrapers in the four crystallizers on the formation and growth of wax crystals is neglected due to their low rotation speeds.
3. Spherical crystals are assumed though plate crystals were observed in most cases (2–4), because this treatment does not affect our discussions. Furthermore, crystal aggregation and loss are neglected.
4. Both wax and oil are looked as pure substances because of their complicated compositions.

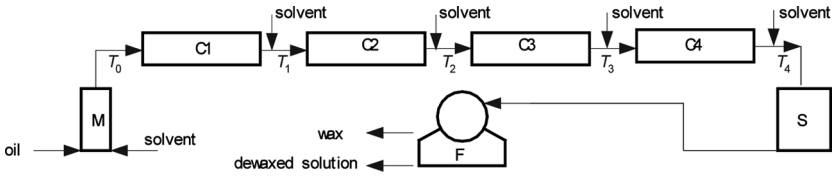

Figure 1. Schematic diagram for a continuous solvent dewaxing process. M: mixing vessel; C1-C4: crystallizers 1-4; S: suspension vessel; F-filter.

It is known that normal paraffins (C_nH_{2n+2} or C_n herein) such as C_{20}-C_{40} are present in high proportion in wax (5,6), among them C_{24}, C_{28}, and C_{32} are the dominant compositions for many cases (3,5). Therefore, it is acceptable to choose one of them as the representative compound of wax. On the other hand, lube base oil usually has a relatively high boiling point and low pour point; it is convenient to choose decane (C_{10}) as the representative compound of DWO, which has a melting point of 243 K and a boiling point of 447 K.

Population Balance Equation (PBE)

Define n ($=\mathrm{d}N/\mathrm{d}L$) as the particle population density function in representative of the number of nuclei per unit volume of solution in the nucleus size interval $\mathrm{d}L$

$$n = \frac{\mathrm{d}N}{\mathrm{d}L} \tag{1}$$

where N is the particle density referring to the number of nuclei with sizes from 0 to L per unit volume. It is known that nucleation triggers from the combination of molecules to reduce the system's free energy. If the size of the formed crystals is less than that of the critical nucleus L_{crit}, they are embryos in a thermodynamically unstable state, and can be dissolved into solution again. If the size of the formed crystals is larger than L_{crit}, the crystals or nuclei will grow up. The Dirac function δ can be applied to describing this discontinuity. Although the fluid velocity u changes following the addition of dewaxing solvent, it is fixed in each crystallizer. As a result, the PBE can be established in an increment $\mathrm{d}z$ along the flow direction in any crystallizer by neglecting crystal aggregation and loss

$$u\frac{\partial n}{\partial z} + \frac{\partial (nG)}{\partial L} = J\delta(L - L_{\mathrm{crit}}) \tag{2}$$

where $J = \mathrm{d}N/\mathrm{d}t$ is the rate of nucleation; G is the growth rate of crystals, which is defined as $\mathrm{d}L/\mathrm{d}t$.

Crystallization Kinetics

In general, the primary and secondary nucleations occur simultaneously, the sum of which is the overall nucleation rate. Relatively, the secondary nucleation requires a low supersaturation because it proceeds on the base of the formed nuclei, which plays an important role for formation of

larger crystals in industrial crystallization. As a compromise, an empirical form (7) is applied to the overall rate of nucleation

$$J = K_n \Delta C^p = K_n C_{\text{sat}}^p (S-1)^p \tag{3}$$

where K_n is the nucleation rate constant; p is the nucleation order; ΔC is the supersaturation of wax in solution; and S is the relative supersaturation. Different supersaturations have the following relationships

$$\Delta C = C - C_{\text{sat}}; \quad S = C/C_{\text{sat}} \tag{4}$$

where C is the true wax concentration in solution; C_{sat} is the equilibrium solubility of wax in solution.

According to the overall mass deposition rate with a first-order growth law (7), the overall linear growth rate can be expressed as

$$G = \frac{k_{\text{d}}}{3\rho_{\text{W}} f_{\text{v}}/f_{\text{a}}} C_{\text{sat}}(S-1) \tag{5}$$

where ρ_{W} is the crystal (wax) density; f_{v} is the crystal's volume shape factor ($\pi/6$ for spherical particles); f_{a} is the crystal's surface shape factor (π for spherical particles); k_{d} is the mass transfer coefficient of wax by diffusion which can be estimated with the Sherwood number $\text{Sh} = k_{\text{d}}L/D$. Because the particle Reynolds number is close to zero due to the small crystal sizes in this study, then $\text{Sh} = 2$. Consequently, equation (5) can be reduced to

$$GL = \frac{4D}{\rho_{\text{W}}} C_{\text{sat}}(S-1) \tag{6}$$

Equation (6) indicates that GL is independent on crystal size, which is required for the moment transformations as will be addressed later. In equation (6), D is the mutual diffusion coefficient of wax in solution. The wax molar fraction in the oil feedstock is about 0.1, and much less than 0.1 follong the addition of dewaxing solvent when assuming that, the solvent could be mixed into the oil. In this case (8), D can be looked as the mutual diffusion coefficient at infinite dilution for a pseud binary system (wax and solvent-oil), and the Wilke-Chang equation (9) is applicable

$$D = 7.4 \times 10^{-15} \frac{T(\zeta M_{\text{m}})^{0.5}}{\eta(\overline{V}_{\text{w}} \times 10^6)^{0.6}} \tag{7}$$

where T is the temperature; $\zeta = 1$ is the association parameter for the unassociated solution; M_{m} is the molar mass of the solvent-oil mixture estimated by the molar masses of oil, MEK, and toluene with their

compositions using the solvent to oil ratio (r_{SD}) and MEK to toluene ratio (r_{MT}); $\overline{V}_W$ is the molar volume of solid wax. By neglecting the interaction of the solvent and oil and assuming a homogenous oil-solvent solution; the solution viscosity η can be estimated with

$$\ln \eta = x_S \ln \eta_S + x_D \ln \eta_D \tag{8}$$

where x_S and x_D are respectively the molar fraction of solvent and oil (decane) in the solution. They can be calculated by the volumetric flow rates (or the solvent to oil ratio r_{SD}) and the densities of solvent and oil. η_D and η_S are respectively the viscosities of oil and solvent, with the latter one being calculated by using the same form of equation (8) under any MEK to toluene ratio (r_{MT}).

PBE's Moment Form

The moment method was employed to solve the PBE in this study because it can be converted into several sets of ordinary differential equations with different orders of moment, and can finally give relatively accurate crystal size information (10).

The jth order moment, m_j, is defined as

$$m_j = \int_0^\infty L^j n(L,z) \mathrm{d}L \tag{9}$$

with $n(\infty, z) = 0$; $n(L, 0) = 0$. As shown in the appendix, using the moments and equation (6), the PBE can be converted into the following equations

$$u\frac{\mathrm{d}m_j}{\mathrm{d}z} = j(GL)m_{j-2} + JL_{\mathrm{crit}}^j \quad (j = 0, 1, 2, 3) \tag{10}$$

with the boundary conditions

$$m_1(0) = m_0(0)L_W;\ m_2(0) = f_a m_0(0)L_W^2;\ m_3(0) = f_v m_0(0)L_W^3 \tag{11}$$

where $m_0(0)$ arbitrarily takes 0.001-1 particle/(m^3s) implying almost no particles at $z = 0$ to comply with $n(L, 0) = 0$; L_W is the size of a single wax molecule calculated by the volume of the molecule (ν). In above equations, the size of the critical nucleus L_{crit} is a function of S(7)

$$L_{\mathrm{crit}} = \frac{2\sigma\nu}{k_B T \ln S} \tag{12}$$

where σ (in N/m) is the interfacial tension between solid (wax) and liquid (solution); k_B is the Boltzmann constant. The volume of a wax molecule

is calculated with

$$\nu = \frac{M_{\mathrm{w}}}{\rho_{\mathrm{W}} N_{\mathrm{A}}} \tag{13}$$

where M_{w} is the wax molar mass, N_{A} is Avogadro's constant. In equation (10), the third moment m_3 is the sum of crystal volumes per unit volume of solution, which can be used to obtain the recovery of precipitated wax in solution, namely, $(\pi/6)m_3(r_4+1)/\phi_0$, being ϕ_0 the wax volume fraction in the oil feedstock and r_4 the solvent to oil ratio at the exit of the fourth crystallizer. According to the lognormal function as will be specified later, m_{-1} in equation (10) can be expressed with other moments

$$m_{-1} = m_2 m_0^3 / m_1^3 \tag{14}$$

Particle Density Function

The moment method has a drawback that the reduced equations are not closed after the moment conversion; an additional assumption on particle distribution should be given before calculation; here, the lognormal function (10,11) is adopted

$$n(L) = \frac{m_0}{\sqrt{2\pi\beta^2}L} \exp\left(-\frac{(\ln L - \alpha)^2}{2\beta^2}\right) \tag{15}$$

where $\alpha = \ln L_a$ is the mathematical expectation of the particle distribution, in which L_a is the average geometrical size; β is the standard variance of the distribution. Substituting equation (15) into equation (9), we have

$$\beta^2 = \ln\left(\frac{m_2 m_0}{m_1^2}\right) \tag{16}$$

$$L_a = \frac{m_1}{m_0 \exp\left(\frac{\beta^2}{2}\right)} \tag{17}$$

Equations (15–17) can detail the information of the wax crystals once the three moments (m_0, m_1, and m_2) have been determined through solving equation (10).

Wax Supersaturation in Solution

In order to solve the PBE, the phase equilibrium data for the wax-oil-solvent system are required for calculating S; a solubility prediction model for non-hydrogen-bonded solvents is adopted (12)

$$\begin{aligned}\ln \phi_{\mathrm{W}i} = &-\frac{\Delta H_{\mathrm{m}}}{R}\left(\frac{1}{T}-\frac{1}{T_{\mathrm{m}}}\right)-\frac{\Delta H_{\mathrm{t}}}{R}\left(\frac{1}{T}-\frac{1}{T_{\mathrm{t}}}\right)\\ &-0.5(1-\phi_{\mathrm{W}i})\left(1-\frac{\overline{V}_{\mathrm{W}}}{\overline{V}_i}\right)\\ &+0.5\ln\left[\phi_{\mathrm{W}i}+(1-\phi_{\mathrm{W}i})\frac{\overline{V}_{\mathrm{W}}}{\overline{V}_i}\right]\\ &-\frac{(1-\phi_{\mathrm{W}i})^2\overline{V}_{\mathrm{W}}}{RT}(\delta_{\mathrm{W}}-\delta_i)^2 (i=\mathrm{D},\mathrm{T},\mathrm{M})\end{aligned} \tag{18}$$

where the subscripts D, T, M refer to decane, toluene, and MEK respectively; R is the universal gas constant; ΔH_{m} and ΔH_{t} are the heat of fusion and transition of wax (J/mol); T_{m} and T_{t} are the wax melting and transition temperatures; δ and $\bar{V}$ represent solubility parameter and molar volume, respectively. ϕ_{W_i} is the volume fraction of wax in liquid i; the corresponding mass fraction $w_{\mathrm{W}i}$ can be calculated with

$$\phi_{\mathrm{W}i}=\frac{\overline{V}_{\mathrm{W}}w_{\mathrm{W}i}/M_{\mathrm{W}}}{\overline{V}_{\mathrm{W}}w_{\mathrm{W}i}/M_{\mathrm{W}}+\overline{V}_i(1-w_{\mathrm{W}i})/M_i}\ (i=\mathrm{D},\mathrm{T},\mathrm{M}) \tag{19}$$

where M refers to molar mass. To avoid the calculations of wax in a multi-component solvent, equations (18) or (19) are used to calculate the solubilities of wax in C_{10}, toluene, and MEK, separately. The last term (the endotherm effect) of equation (18) is not needed for the solubility of wax (C_{24}, C_{28}, or C_{32}) in C_{10} (12). The modified solubility parameters are used in equation (18) for improving the prediction of the solubilities of wax in toluene or MEK (12).

The equilibrium solubility of wax in the wax-oil-solvent solution can be expressed as

$$C_{\mathrm{sat}}=\frac{\sum w_{\mathrm{W}i}\rho_i\dot{V}_i}{\dot{V}_{\mathrm{total}}}=\frac{w_{\mathrm{WD}}\rho_{\mathrm{D}}}{1+r_{\mathrm{SD}}}+\frac{r_{\mathrm{SD}}(w_{\mathrm{WT}}\rho_{\mathrm{T}}+r_{\mathrm{MT}}w_{\mathrm{WM}}\rho_{\mathrm{M}})}{(1+r_{\mathrm{SD}})(1+r_{\mathrm{MT}})} \tag{20}$$

where, as before, ρ denotes density; $\dot{V}$ refers to volumetric flow rate. $\dot{V}_{\mathrm{total}}$ is the overall oil-wax-solvent solution volumetric flow rate ($\dot{V}_{\mathrm{total}}=\dot{V}_{\mathrm{S}}+\dot{V}_{\mathrm{D}}=\dot{V}_{\mathrm{M}}+\dot{V}_{\mathrm{T}}+\dot{V}_{\mathrm{D}}$); $\dot{V}_{\mathrm{S}}$ is the solvent volumetric flow rate; $r_{\mathrm{SD}}=\dot{V}_{\mathrm{s}}/\dot{V}_{\mathrm{D}}$ is the solvent to oil ratio; $r_{\mathrm{MT}}=\dot{V}_{\mathrm{M}}/\dot{V}_{\mathrm{T}}$ is the MEK to toluene ratio. The true solute concentration C in the

wax-oil-solvent solution can be calculated by

$$C = (\rho_W \phi_0 \dot{V}_D - \rho_W f_v m_3 \dot{V}_{total})/\dot{V}_{total} = \rho_W \phi_0/(1 + r_{SD}) - \rho_W f_v m_3 \quad (21)$$

where ϕ_0 is the volume fraction of wax in the oil feedstock.

Temperature Distribution in Crystallizers

When operating the pilot-plant, the exit and inlet temperatures of each crystallizer were automatically controlled, so it is convenient to assume a linear temperature distribution in each crystallizer. Letting $T_{i\text{-}1}$ and T_i be the inlet and outlet temperatures of the ith crystallizer (see Fig. 1), the cooling rate for the crystallizer is

$$\frac{\Delta T}{Z} = \frac{T_{i-1} - T_i}{Z} \quad (i = 1, 2, 3, 4) \quad (22)$$

where Z is the crystallizer's length. From equation (22), the temperature at any position z of the ith crystallizer along the flow direction can be calculated with

$$T(z) = T_{i-1} + z\frac{\Delta T}{Z} \quad (23)$$

MODELING RESULTS AND DISCUSSION

Source of Data and Specifications

Equation (10) involves four sets of ordinary differential equations, which can be solved by using the Runge-Kutta-Fehlberg algorithm (13); the FORTRAN language was used to implement all the calculations. Before the calculation, many fundamental data are required, including the crystallizer dimensions, operating conditions, physical properties of oil and wax compounds, and the thermodynamics and kinetics data of the complicated system. They are specified separately as follows.

The four crystallizers were connected in series; each crystallizer has a length of $Z = 0.8$ m. A scheme was arranged with decreasing inner volumes from the first to the fourth crystallizer: 1.11, 0.946, 0.769, and 0.579 L. The oil flow rate was fixed at 1 L/h ($\dot{V}_o = 0.001\ m^3/h$) with an initial wax content of 0.3083 (ϕ_0). This value is for the Oman #3 distillate from a vacuum distillation column in Maoming Petroleum Corporation, China. Normally, the premixing ratio of solvent to oil was 0.5:1, namely, $r_{SD} = r_0 = 0.5$; the solvent to oil ratio in each crystallizer (r_{SD})

is equal to the solvent-to-oil ratio at the exit of the ith crystallizer (r_i), which can be determined according to the dilution solvent added between the first and the fourth crystallizers. The average velocity of the wax-oil-solvent mixture flowing in each crystallizer can be calculated according to the crystallizer dimensions and the flow rates of the mixture. The MEK to toluene ratio (r_{MT}) for the dewaxing solvent is 1:1 if there is no further specification. The interfacial tension σ for C_{24} between its solid and liquid states is equal to 0.0082 N/m, which is also adopted for that of C_{28} and C_{32}, as it indicated that the interfacial tensions of C_{17}, C_{18}, and C_{24} have no big difference (14). C_{10}'s viscosity (used as the oil viscosity) in the temperature range 283–423 K is expressed as (15).

$$\eta_0 = 8.498 \times 10^{-4} \exp\left[-7.1561 + \frac{14.2582}{T/298.15} - \frac{11.396}{(T/298.15)^2} + \frac{4.2942}{(T/298.15)^3}\right] \quad (24)$$

The viscosity data of MEK and toluene at different temperatures are listed in Table 1; the table also provides the density data of toluene and C_{10} from the NIST free database. The MEK's density in the temperature range 278–323 K was reported elsewhere (16). The solid densities of wax (C_{32}, C_{28}, and C_{24}), the modified solubility parameters of MEK and toluene, the values of ΔH_m, ΔH_t, T_m, and T_t used in equation (18) could be found in reference (12).

Taggart et al. (17) reported that the nucleation rate constants and nucleation orders of n-alkanes from C_{13} to C_{32} in the case of heterogeneous nucleation in stagnant melts. The nucleation orders, i.e., 5.2 for C_{24}, 2.8 for C_{28}, and 1.6 for C_{32}, were approximately adopted in this study because they used an expression of nucleation rate similar to equation (3), but the K_n values could not be directly applied because a mass nucleation rate was specified in the reference. Instead, K_n is looked as an

Table 1. Physical properties of MEK, toluene, and decane (C_{10}) at different temperatures

	Temperature, K			
Physical properties	248	273	298	323
Viscosity of MEK, mPa.s	0.720	0.533	0.405	0.315
Viscosity of toluene, mPa.s	1.165	0.778	0.560	0.424
Density of toluene, kg/m^3	908.59	885.49	862.30	838.82
Density of Decane, kg/m^3	765.66	746.02	726.56	707.10

adjusted parameter that can be obtained from experimental information. In later simulations, different K_n were used in order to ensure a reasonable comparison under different operating conditions. It will also be further discussed that the effects of K_n and p on the simulated wax crystals.

The calculated solublities (ϕ_{WD}) of C_{24}, C_{28}, and C_{32} in decane from equation (18) are respectively 0.447, 0.244, and 0.00878 at 313 K. The solid wax disappeared (solid wax is dissolved, not melted) when heating the Oman #3 distillate to about 313 K, indicating that the solubility of wax in oil should be larger than $\phi_0 = 0.3083$. Therefore, C_{24} as the wax compound is a suitable choice.

The Effect of Temperature Distribution

The temperature distribution in crystallizers determines the cooling rate of the feed mixtures, and then affects the nucleation rate and growth rate via changing the supersaturation of wax compounds in solution. In order to look into this effect, three temperature distributions in the four crystallizers were designed as TI, TII, and TIII, in which TIII has a low cooling rate in the first and second crystallizers, but a high cooling rate in the fourth crystallizer. Table 2 shows these modes and details the calculated average crystal size L_a, supersaturation S, and the third moment m_3 at the exits of the four crystallizers ($z = 0.8$ m, 1.6 m, 2.4 m, 3.2 m) with a solvent-to-oil ratio designed as RV (see Table 3). Figure 2 gives the simulated CSDs at the exit of the fourth crystallizer under different cooling

Table 2. Temperature distributions and their effects on the simulated wax crystals ($T_0 = 313$ K; $K_n = 5 \times 10^{-6}$; $P = 5.2$)

	z (m)	0.8	1.6	2.4	3.2
	r_1-r_4 (RV)	0.5	0.5	1.5	1.5
TI	T_1-T_4 (K)	293	273	268	258
	L_a (μm)	206	401	549	614
	S	4	45	69	278
	m_3 (m^3/m^3)	0.0	0.035	0.058	0.074
TII	T_1-T_4 (K)	298	278	268	258
	L_a (μm)	157	352	526	594
	S	2	24	78	321
	m_3 (m^3/m^3)	0.0	0.018	0.036	0.049
TIII	T_1-T_4 (K)	303	293	278	258
	L_a (μm)	83	270	451	469
	S	1	4	23	392
	m_3 (m^3/m^3)	0.0	0.001	0.005	0.007

rates, in which the y-axis is a combination of the crystal population density function $n(L)$ with L and m_0.

As Table 2 shows, L_a, S, and m_3 increase along the flow direction under all investigated temperature distributions. The supersaturation has a dramatic increase due to the fast decrease of the equilibrium concentration of wax in the solution, resulting in a considerable crystal formation and growth. From the calculated m_3 data, the recoveries of wax at the exit of the fourth crystallizer are 31, 21, and 3% with respect to the cases of TI, TII, and TIII, respectively. As shown in Fig. 2a, relatively small crystals are produced under the temperature distribution of TIII; this is because that smaller cooling rate at the beginning of the crystallization brings smaller supersaturation of wax in solution, leading to lower crystal growth and crystal formation rate. However, this conclusion depends also on the wax compounds adopted, for example, the simulated average crystal sizes are 597, 598, and 616 μm with respect to the cases of TI, TII, and TIII (RV, $K_n = 1$ (particles/m^{3}s)/(kg/m^3)$^{2.8}$), respectively, if the wax is C_{28}. Therefore, different systems should use different operating temperature distributions, although it is empirically known that a smaller cooling rate at the early stage of crystallization following a higher cooling rate later can improve crystal sizes.

In addition, it is also necessary to choose an appropriate preheating temperature (T_0) and a feasible exit temperature (T_4) in a practical dewaxing process. Figure 2b shows the effect of T_0 on CSDs (other temperatures follow TI). It indicates that a low T_0 will slightly increase the crystal sizes and broaden the CSDs, though the CSDs and crystal sizes are very close under $T_0 = 313$ K and $T_0 = 303$ K. As far as T_4 is concerned, both the crystal size and the crystal quantity (indicated as the recovery of wax) show no big difference under $T_4 = 243$–263 K; this is also true for C_{28} and C_{32}. It reveals that a further decrease of T_4 is not significant for crystal growth, but a suitable arrangement of the temperature distribution is still important because here T_3 is relatively low (it will be further addressed later when discussing Table 4). In a dewaxing process, T_0 ($>$ ambient temperature) and T_4 (<273 K) are the highest and lowest operating temperatures, respectively; it is possible to achieve desired crystal sizes and reduce energy consumption by using a relatively low T_0 and a relatively high T_4.

The Effect of Multiple Dilution Operation

In the model, equations (8), (20), and (21) can reflect the effect of multiple dilution operation, which show that the addition of solvent affects the supersaturation of wax in solution, the solution's physical properties, and the flow's hydrodynamic behavior.

Because many multiple dilution operations could be arranged for a four-crystallizer dewaxing process, Table 3 shows some typical schemes designed as RI-RVI. In the case of RI, $r_1 = 0$ means that the premixing solvent-to-oil ratio is zero, and it is the same in the first crystallizer. $r_2 = 0.5$ means that 0.5 L/h dilution solvent with temperature T_1 is added after the first crystallizer but before the second crystallizer. $r_3 = 1.0$ denotes that a second stream of 0.5 L/h dilution solvent with temperature T_2 is added after the second crystallizer and before the third crystallizer. $r_4 = 1.5$ represents that a third stream of 0.5 L/h dilution solvent with temperature T_3 is added after the third crystallizer and before the fourth crystallizer. Consequently, RI refers to three additions of the dilution solvent but without the premixing solvent; RII, RIII, and RIV denotes two additions of the dilution solvent with different premixing solvent; RIV, RV, and RVI represents two additions of the dilution solvent with adding the second streams into different crystallizers (positions).

Figure 3 shows the simulated CSDs at the exit of the fourth crystallizer under different multiple dilution operations, revealing that the operations play an important role on the crystal formation and crystal growth. Figure 3a shows that the produced wax crystals from RI have the largest average size, largest quantity with a relatively narrow CSD ($L_a = 756\,\mu m$, $y = 80\%$, $\beta = 0.25$), corresponding to the case of zero premixing solvent flow rate. However, the wax crystals obtained from RIV have the smallest average size, smallest quantity, and broadest CSD ($L_a = 454\,\mu m$, $y = 3\%$, $\beta = 0.47$), corresponding to the largest premixing solvent flow rate. The results from RII show that few crystals with small crystal sizes and relatively narrow CSD ($\beta = 0.21$) are obtained compared to that from RI. It may conclude that the lower premixing solvent flow rate tends to produce more crystals with larger crystal sizes because of the relatively long residence time in the first crystallizer for

Table 3. Different multiple dilution schemes

Z (m)		0.8	1.6	2.4	3.2
T_1-T_4 (K)		293	273	268	258
RI	r_1-r_4	0	0.5	1.0	1.5
RII	r_1-r_4	0.1	1.5	1.5	1.5
RIII	r_1-r_4	0.3	1.5	1.5	1.5
RIV	r_1-r_4	0.5	1.5	1.5	1.5
RV	r_1-r_4	0.5	0.5	1.5	1.5
RVI	r_1-r_4	0.5	0.5	0.5	1.5

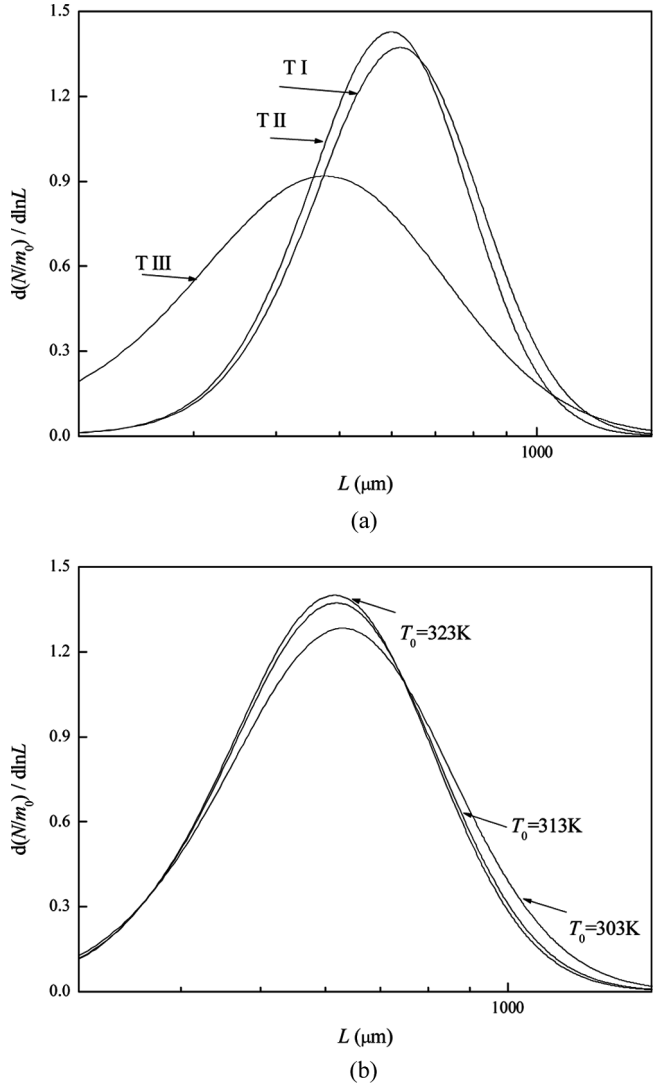

Figure 2. Effect of cooling rates (a) and T_0 (b) on CSDs (multiple dilution: RV; $K_n = 5 \times 10^{-6}$; $p = 5.2$).

wax crystal formation and growth. Comparisons of the curves in Fig. 3b under RIV, RV, and RVI reveal that a late addition of dilution solvent has benefit to crystal's further formation and growth ($L_a = 618\,\mu m$, $y = 56\%$, $\beta = 0.36$ with respect to RVI; $L_a = 454\,\mu m$, $y = 3\%$,

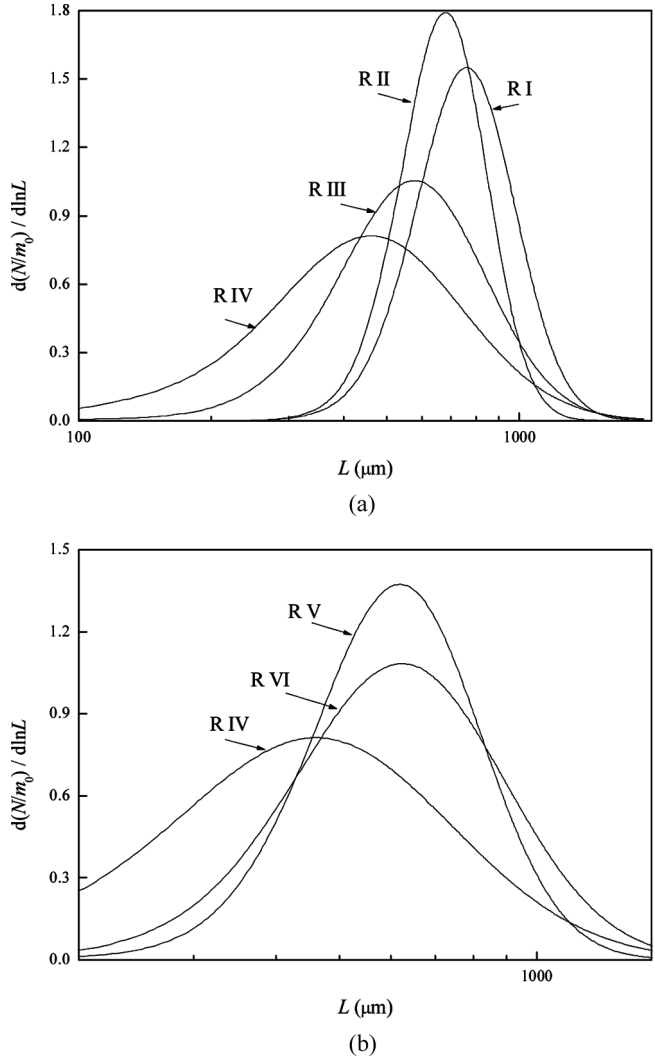

Figure 3. Effect of the multiple dilution operations on CSDs (temperatures: TI; $K_n = 5 \times 10^{-6}$; $p = 5.2$). The multiple dilution schemes (RI-RVI) for adding dewaxing solvents are shown in Table 3.

$\beta = 0.47$ with respect to RIV). It can also be observed that an appropriate addition of the dilution solvent can achieve a narrow CSD such as the case of RV ($\beta = 0.27$). As tested, the above conclusions are also available for C_{28} and C_{32}.

The Effect of MEK to Toluene Ratio

It is commonly known that increasing MEK in the MEK/toluene solvent has benefit to the wax crystallization and filtration, and then improve the recovery of wax because of its low viscosity and polar nature. On the other hand, increasing toluene in the mixture solvent can increase the recovery of DWO because of its low polarity. It is interesting to examine the effect of the composition of the dewaxing solvent on the formed wax crystals based on the model, which is expressed in the calculation of the diffusion coefficient and solubility of wax in solution. Using $K_n = 5 \times 10^{-6}$ (particles/m^{3}s)/(kg/m^3)$^{5.2}$, the calculations under RV and T1 show that $L_a = 605\,\mu m$, $y = 29\%$, $\beta = 0.27$ when the solvent is a pure toluene; $L_a = 613\,\mu m$, $y = 31\%$, $\beta = 0.27$ when the MEK to toluene ratio is 0.5; and $L_a = 621\,\mu m$, $y = 34\%$, $\beta = 0.27$ when it is a pure MEK. As it shows, the higher content of MEK in the dewaxing solvent is beneficial to producing larger amount of crystals with relatively larger sizes. It is because the diffusion coefficient of wax in MEK ($D = 5.07$–$10.8 \times 10^{-10}\,m^2/s$) is larger than that in toluene ($D = 3.87$–$9.68 \times 10^{-10}\,m^2/s$) under the calculation conditions, and that the solubility of wax in MEK is much less than that in toluene: $\phi_{WM} = 0.00132$ and $\phi_{WT} = 0.432$ at 313 K calculated by equation (18) for C_{24}. As far as C_{28} or C_{32} is concerned, the effect of the MEK to toluene ratio on crystals becomes more obvious, and the above conclusion from C_{24} is still hold.

The Effects of Other Factors

In a solvent dewaxing process, the temperature distribution and the multiple dilution operation are two key operating conditions. On the other hand, the system's characteristics may also consumedly affect the process, among them, the nucleation constant, the nucleation order, and the wax compound will be discussed in this section since the system is too complicated to exactly determine these data. Furthermore, the crystallizer dimensions will be addressed to examine the scheme with decreasing inner volumes from the first to the fourth crystallizer.

Figure 4a shows that a low K_n increases the crystal sizes and slightly narrows the CSDs, but clearly decreases the formed crystal quantity ($y = 8\%$ when $K_n = 10^{-6}$(particles/m^{3}s) (kg/m^3)$^{5.2}$; $y = 90\%$ when $K_n = 5 \times 10^{-6}$ (particles/m^{3}s)/(kg/m^3)$^{5.2}$. Figure 4b indicates that p does not have an obvious effect on CSDs, but a high p can slightly reduces the crystal sizes, and dramatically increase the crystal quantity ($y = 2\%$ when $p = 4.5$; $y = 69\%$, when $p = 5.5$). Hence, both K_n and p are sensitive to the recovery of wax.

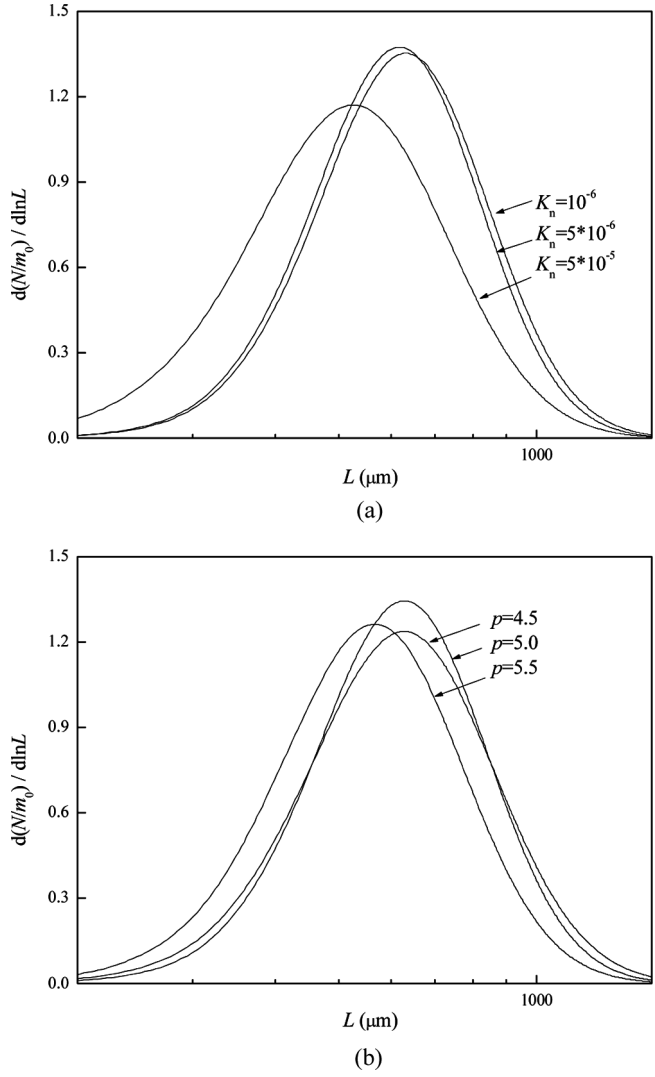

Figure 4. Effect of parameters K_n ($p = 5.2$) and p ($K_n = 5 \times 10^{-6}$) on CSDs (operating conditions: TI, RV).

Figure 5 shows the effects of different wax compounds on the simulated CSDs and crystal sizes. Figure 5a shows that for C_{24} a large number of crystals with small sizes and narrow CSD ($L_a = 499\,\mu m$, $y = 97\%$, $\beta = 0.32$) are produced. However, very few crystals with broad CSD

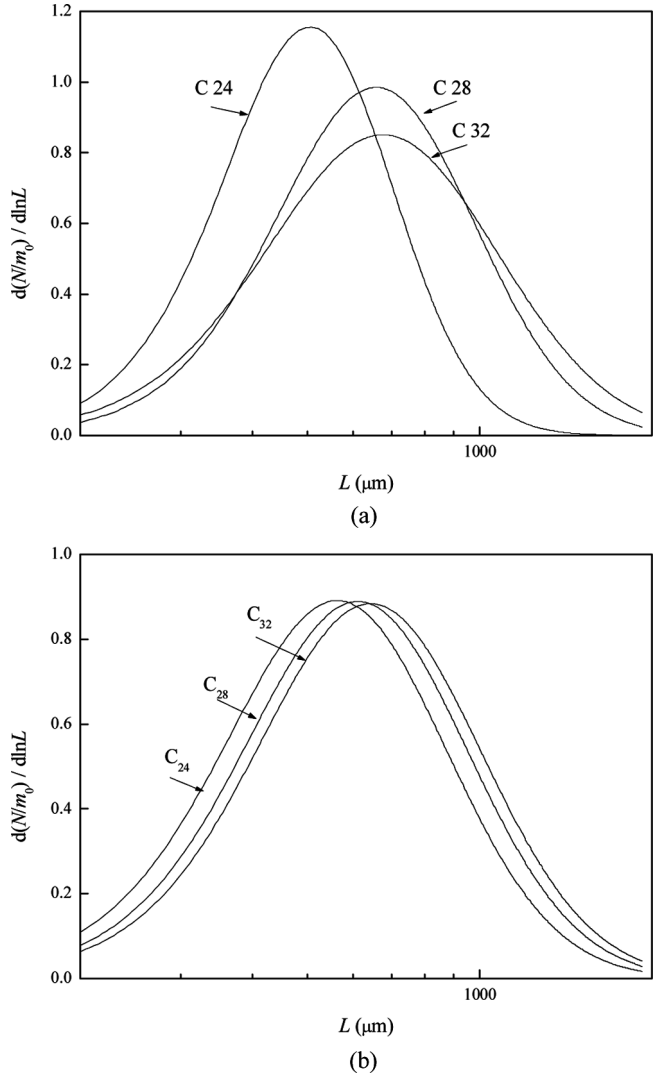

Figure 5. Effect of the wax compounds on CSDs (operating conditions: TI and RV): (a) $K_n = 8 \times 10^{-5}$, $p = 1.6$, 2.8 and 5.2 for C_{32}, C_{28} and C_{24}, respectively; (b) $K_n = 100$, $p = 1.6$.

and large sizes ($L_a = 672\,\mu m$, $y = 0.0\%$, $\beta = 0.42$) are produced in the case of C_{32}, revealing that wax crystal formation significantly depends on the compositions of wax. For a further comparison, $p = 1.6$ is assumed to be identical for any wax compounds (in this case a large

K_n should be used to avoid forming very few crystals in particular for C_{24}); it can be observed from Figure 4b, that fewer crystals and smaller crystal sizes ($L_a = 558\,\mu m$, $y = 28\%$, $\beta = 0.44$) are obtained for C_{24} in comparison with C_{32} ($L_a = 639\,\mu m$, $y = 62\%$, $\beta = 0.44$). This reveals that the physical properties of wax are of concern because they can influence the supersaturation of wax in solution through equations (18) and (19), and finally influence the wax crystals.

Finally, different crystallizer dimensions designed as CI (0.4, 0.6, 0.8, and 1.0 L for the first to the fourth crystallizer, respectively), CII (0.7L for each crystallizer), and CIII (1.0, 0.8, 0.6, and 0.4 L for the first to the fourth crystallizer, respectively) are examined. Using $K_n = 5 \times 10^{-6}$ (particles/m^{3}s)/(kg/m^3)$^{5.2}$, the calculations under RV and T1 indicate that the crystals from CIII have the largest quantity, smallest average size, and broadest CSD ($L_a = 611\,\mu m$, $y = 20\%$, and $\beta = 0.22$ for CI; $L_a = 554\,\mu m$, $y = 21\%$, and $\beta = 0.29$ for CIII). This becomes more obvious, and even a reverse trend of L_a can be observed if the wax compound is C_{32} with $K_n = 100$ (particles/m^{3}s)/(kg/m^3)$^{1.6}$ ($L_a = 524\,\mu m$, $y = 25\%$, and $\beta = 0.44$ for CI; $L_a = 600\,\mu m$, $y = 49\%$, and $\beta = 0.45$). Therefore, the arrangement of CIII is feasible for a practical operation due to forming a large number of crystals, and in some cases, of large crystals.

COMPARISON WITH EXPERIMENTAL RESULTS

Because K_n is an undetermined parameter in the model, it can be obtained by matching calculated data to available experimental information such as crystal sizes or CSDs. Although some SEM images of wax crystals were reported in a previous work (2), it is still difficult to estimate the crystal sizes and CSDs due to the bridged and agglomerated wax crystals. However, the wax recovery can be applied to fitting K_n since the former is sensitive to the latter as indicated from the simulations. An experimental wax recovery, $y_{exp} = 62.7\%$ (see Table 4) that was averaged from three repeated experiments under the same operating conditions with a maximum difference of 9.1% (2) was used to fit the calculated recoveries. $K_n = 0.00344$ (particles/m^{3}s)/(kg/m^3)$^{5.2}$ ($p = 5.2$) for C_{24}, $K_n = 4.25$ (particles/m^{3}s)/(kg/m^3)$^{2.8}$ for C_{28} ($p = 2.8$), and $K_n = 227$ (particles/m^{3}s)/(kg/m^3)$^{1.6}$ for C_{32} ($p = 1.6$) were obtained. K_n was computed from the objective function $|1 - y_{cal}/y_{exp}| < 10^{-3}$ (y_{cal} is the calculated wax recovery from the proposed model) either by manual variation of K_n or any one-dimension optimizing program such as golden section search (13). For different wax compounds, different p values and physical properties should be used to obtain K_n.

Table 4. Comparisons of experimental recoveries of wax with calculated results ($T_0 = 313$ K; $r_1 = 0.5$; $r_2 = r_3 = r_4 = 1.5$)

T_1-T_4 (K)	MEK/toluene ratio	y_{exp}	y_{cal}/L_a [b]	y_{cal}/L_a [c]	y_{cal}/L_a [d]
301, 288, 283, 278	2:3	62.7[a]	62.7/399	62.7/555	62.7/609
301, 278, 268, 263	2:3	82.4	75.5/381	58.9/517	58.6/577
301, 278, 268, 263	1:1	92.6	77.5/388	61.6/528	60.5/584
301, 278, 268, 263	3:2	96.3	79.4/389	64.1/538	62.2/591

[a]It was used to determine K_n; [b]C_{24}; [c]C_{28}; [d]C_{32}; L_a in μm.

Table 4 presents the predicted or calculated recoveries of wax (y_{cal}) along with the average crystal sizes at the exit of the fourth crystallizer under other operating conditions by using the fitted K_n for all the three wax compounds. As the table shows, the predicted recoveries for C_{24} are in acceptable agreement with the experimental data under different MEK to toluene ratios, although the predictions are underestimated. The y_{exp} in Table 4 were not directly from the experiments, but obtained from the recoveries of DWO (2); in the calculation, an average oil content (12%) in the filtrated slack wax-oil mixture was deducted, assuming that there is no loss of oil in the oil-solvent separation and filtration processes. The underestimation of the predications can be partly attributed to this assumption and the neglecting of the crystal growth in the suspension vessel. Comparison of the first and the second lines in Table 4 shows that an appropriate arrangement of T_1-T_4 with a low T_4 can truly improve the wax removal from the waxy oil when using the wax compound C_{24}. However, for the C_{28}-C_{10} or C_{32}-C_{10} system, reverse results can be observed, indicating again that C_{24} is a more suitable choice as the main representative wax compound.

CONCLUSIONS

In this work, a steady 1-D parallel flow model was established for the solvent dewaxing process based on the particle population balance, crystallization kinetics, phase equilibrium, and the nature of the tube-in-tube crystallizer. Using this model, the effect of operating conditions (temperature distributions, multiple dilutions and the MEK to toluene ratio), system's characteristics (nucleation kinetics parameters and wax compound), and the crystallizer dimensions on the formed wax crystals is simulated and discussed in detail. From these studies, conclusions under the investigated conditions are as follows:

1. A relatively small cooling rate at the beginning of crystallization and a relatively high cooling rate at the late stages of the crystallization

provide few crystals with small sizes at the exit of the fourth crystallizer; reverse results may be achieved when using different wax compounds.
2. It is possible to use a relatively low premixing temperature of the oil feedstock-solvent mixture and a relatively high exit temperature of the fourth crystallizer to achieve desired wax crystals and reduce the process energy consumption simultaneously.
3. Multiple dilution operation has a very effective effect on the wax crystal formation and growth. A low premixing solvent flow rate is beneficial to forming a large number of crystals with large sizes and narrow CSDs. A late addition of dilution solvent is helpful to produce a large number of crystals with large sizes.
4. High content of MEK in the MEK/toluene dewaxing solvent is beneficial to producing a large number of crystals with large sizes.
5. The recovery of wax-from-oil feedstock is sensitive to nucleation constant; a low nucleation constant can increase the sizes of wax crystals, but dramatically reduces the formed crystal quantity.
6. A high nucleation order dramatically increases the formed crystal quantity and slightly reduces the crystal sizes. If C_{24} is looked as the wax compound, smaller crystals are produced in comparison with C_{32} or C_{28}. The four crystallizers designed with a decreasing inner volume can increase the formed crystal quantity.
7. The predicted recoveries of wax are in acceptable agreement with available experimental data, which supports that C_{24} could be the main representative wax compound for the investigated distillate. It also indicates that the model could be used to direct the dewaxing operation and process design.

In addition, the established model can also be applied to other continuous crystallization processes using tube-in-tube crystallizers. Nevertheless, before the model's practical applications, it is important to have the system's exact compositions and determine the system's crystallization kinetics parameters by comparing modeling results with more experimental data, such as real time CSDs or crystal sizes at the exit of the final crystallizer.

ACKNOWLEDGMENTS

For financial support, the authors are grateful to the NSFC (Project 20406015), the NCET Program and the NSF of Fujian Province (Project E0710026).

LIST OF SYMBOL

C:	solute concentration in solution, kg/m^3
ΔC:	supersaturation
D:	diffusion coefficient of wax in solution, m$_2$/s
f_v, f_a:	volume/surface shape factor
g:	order of crystal growth
G:	crystal growth rate, m/s
ΔH_m:	heat of fusion, J/mol
ΔH_t:	heat of transition, J/mol
J:	nucleation rate, particles/(m^{3}s)
k_B:	Boltzmann's constant, J/K
k_d:	mass transfer coefficient, m/s
K_n:	nucleation rate constant, (particles/m^{3}s)/(kg/m^3)^p
L:	crystal size, μm
L_a:	average geometrical size, μm
m_0:	zeroth moment, particles/m^3
m_1:	first moment, m/m^3
m_2:	second moment, m^2/m^3
m_3:	third moment, m^3/m^3
M:	molar weight, kg/mol
N:	particle density, particles/m^3
N_A:	Avogadrós constant, molecules/mol
n:	particle size distribution function, particles/(m m^3)
p:	order of nucleation
r_i:	solvent to oil ratio at the exit of the ith crystallizer
r_{SD}:	solvent to oil ratio
r_{MT}:	MEK to toluene ratio
R:	ideal gas constant, J/(K mol)
S:	relative supersaturation
Sh:	Sherwood number, $= k_d L/D$
T:	temperature, K
T_m, T_t:	melting/transition temperature, K
t:	time, s
u:	fluid velocity, m/s
V:	crystallizer volume, m^3
$\dot{V}$:	volumetric flow rate, m^3/h
$\bar{V}$:	molar volume, m^3/mol
v:	molecule's volume, m^3
w:	mass fraction
x:	molar fraction
y:	recovery of wax crystals
Z:	length of crystallizer, m
z:	axial distance, m

Greek Letters

α:	mathematical expectation of particle distribution
β:	standard variance of particle distribution
δ:	solubility parameter, $Pa^{-0.5}$
ϕ:	volume fraction
ρ:	density, kg/m^3
σ:	interfacial tension, N/m
η:	viscosity, Pa s
ζ:	association factor

Subscripts

D:	oil (decane)
M:	MEK
m:	mixture of solvent and oil
s:	solvent
T:	toluene
w:	wax
crit:	critical nuclei
sat:	saturation
0:	feed
1,2,3,4:	exit of the first, second, third and fourth crystallizers

APPENDIX: DERIVATION OF EQUATION (10)

Multiplied by L^j and integrated with respect to L on both sides, equation (2) gives

$$\int_0^\infty u\frac{\partial n}{\partial z}L^j dL + \int_0^\infty \frac{\partial(nG)}{\partial L}L^j dL = \int_0^\infty J\delta(L - L_{\text{crit}})L^j dL \qquad \text{(A1)}$$

According to equation (9), the first term of equation (A1) can be reduced to

$$\int_0^\infty u\frac{\partial n}{\partial z}L^j dL = u\frac{d}{dz}\int_0^\infty nL^j dL = u\frac{dm_j}{dz} \qquad \text{(A2)}$$

where the velocity u is a constant. Because GL is independent on L as indicated in equation (6), the second term of equation (A1) can be written as

$$\begin{aligned}\int_0^\infty \frac{\partial(nG)}{\partial L}L^j dL &= nGL^j\big|_0^\infty - \int_0^\infty jnGL^{j-1}dL \\ &= -jGL\int_0^\infty nL^{j-2}dL = -jGLm_{j-2}\end{aligned} \qquad \text{(A3)}$$

where $n(\infty, z) = 0$ has been applied. According to the property of the Dirac function, the third term of equation (A1) becomes

$$\int_0^\infty J\delta(L - L_{\text{crit}})L^j dL = JL_{\text{crit}}^j \tag{A4}$$

Combing equations (A1–A4), equation (10) can be obtained.

REFERENCES

1. Li, J., Su, Y.Z., Gao, H.Q. (2006) Modeling of the furfural refining process. *Petrol. Sci. Tech.*, *24*: 1347–1356.
2. He, H., Su, Y.Z., Tan, S., Li, J., Gao, H.Q. (2005) A pilot plant for study of solvent dewaxing. *J. Xiamen Univ.* (in Chinese), *44*: 390–395.
3. Imai, T., Nakamura, K., Shibata, M. (2001) Relationship between the hardness of an oil-wax gel and the surface structure of the wax crystals. *Colloid Surf. A: Physicochem. Eng. Asp.*, *194*: 233–237.
4. Kane, M., Djabourov, M., Volle, J.L., Lechaire, J.P., Frebourg, G. (2003) Morphology of paraffin crystals in waxy crude oils cooled in quiescent conditions and under flow. *Fuel*, *82*: 127–135.
5. Dirand, M., Chevallier, V., Provost, E.K.M., Bouroukba, M., Petitjean, D. (1998) Multicomponent paraffin waxes and petroleum solid deposits: Structural and thermodynamic state. *Fuel*, *77* (12): 1253–1260.
6. Srivastava, S.P., Saxena, A.K., Tandon, R.S., Shekher, V. (1997) Measurement and prediction of solubility of petroleum waxes in organic solvents. *Fuel*, *76*: 625–630.
7. Mullin, J.W. (1992) *Crystallization*; 3rd ed.; Butterworth Heinmann: Oxford.
8. Li, J., Hu, X.H., Su, Y.Z., Li, Q.B. (2007) Modeling of a packed bed electrochemical reactor for producing glyoxylic acid from oxalic acid. *Chem. Eng. Sci.*, *62*: 6784–6793.
9. Wilke, C.R., Chang, P. (1955) Correlation of diffusion coefficients in dilute solutions. *AIChE J.*, *1*: 264–270.
10. Li. J., Rodrigues, M., Paiva, A., Matos, H., de Azevedo, E.G. (2005) Modeling of the PGSS process by crystallization and atomization. *AIChE J.*, *51*: 2343–2357.
11. Pratsinis, S.E. (1988) Simultaneous nucleation, condensation, and coagulation in aerosol reactors. *J. Colloid & Interf. Sci.*, *124*: 416–427.
12. Claire, M., Pirson, H., Huys, G., Vanstraelen, E. (1987) New predictive equation for the solubility of solid n-Alkanes in organic solvents. *Ind. Eng. Chem. Res.*, *26*: 447–452.
13. Press, W.H.; Teukolsky, S.A.; Vetterling, W.T.; Flannery, B.P. (1992) *Numerical Recipes*; 2nd ed.; Cambridge University Press.
14. Turnbull, D., Cormia, R.L. (1961) Kinetics of crystal nucleation in some normal alkane liquids. *J. Chem. Phys.*, *34* (3): 820–831.
15. Dymond, J.H., Oye, H.A. (1994) Viscosity of selected liquid n-alkane. *J. Phys. Chem. Ref. Data*, *23*: 41–53.

16. Baraldi, P., Giorgini, M.G., Manzini, D., Marchetti, A., Tassi, L. (2002) Density, refractive index, and related properties for 2-MEK + n-hexane binary mixtures at various temperatures. *J. Solution. Chem.*, *31*: 873–893.
17. Taggart, A.M., Voogt, F. (1996) An examination of the nucleation kinetics of n-alkanes in the homologous series $C_{13}H_{28}$ to $C_{32}H_{66}$, and their relationship to structural type, associated with crystallization from stagnant melts. *Langmuir*, *12*: 5722–5728.